Int. J. Advanced Design and Manufacturing Technology, 2023, Vol. 16, No. 1, pp. 1-11

DOI: 10.30486/ADMT.2022.1939798.1313 *ISSN: 2252-0406* *https://admt.isfahan.iau.ir*

Effect of Adding a Styrene-Butadiene Rubber Damper to A Sled Sample and Extraction of Its Equivalent Stiffness and Damping

Mohammad Reza Najafi [1]
Department of Mechanical Engineering,
University of Imam Hossein comprehensive, Iran
E-mail: drmrnajafi@ihu.ac.ir

Saeed Mahjoub Moghadas [2, *]
Department of Mechanical Engineering,
University of Imam Hossein comprehensive, Iran
E-mail: smahjoubmoghadas@ihu.ac.ir
*Corresponding author

Received: 7 September 2021, Revised: 20 November 2021, Accepted: 26 November 2021

Abstract: Protection of sled systems from destructive vibrations is inevitably under attraction due to the importance of sled testing in the aerospace industry. A pair of SBR dampers were used between the slipper and the sled body to reduce vertical vibrations, so a design of the sled model was studied. Both equivalent stiffness and equivalent damping of the sled system were obtained to reduce the transmission of vibrations from slippers to the body. A combination of analytical, numerical and experimental test methods was utilized and the results were validated. The stiffness values of 370500 and 391000 N/m were obtained from numerical and experimental measurements, respectively. Finally, by designing the sled model, first and second natural frequencies of 12.49 and 19.56 Hz and mode shapes of the sled system were obtained. The results show that the dampers used in the sled have an important role in reducing the transmission of vibrations to the sled body by withstanding the tension and pressure on the slippers.

Keywords: Damper, Equivalent Stiffness, Equivalent Damping, Natural Frequency, Sled Test

Biographical notes: Mohammad Reza Najafi received his Ph.D. in Mechanical Engineering from Imam Hossein comprehensive University, Iran in 2022. His current research interests include vibration and dynamics. **Saeed Mahjoub Moghadas** is an Associate Professor of Mechanical Engineering at Imam Hossein comprehensive University since 1986, Iran. He has received a doctorate with the thesis subject to “Internal Combustion Engines Control and Diagnostics through Instantaneous Speed of Rotation Analysis” at L'ensam university in Paris, France, in 1985. He has authored 20 books and translated 15 others in the field of dynamic, vibration, and control.

Research paper

1 INTRODUCTION

Today, several tests in the aerospace industry are designed and performed using a sled system. This technology is used to achieve supersonic velocities and is widely applicable in space equipment testing [1], projectile penetration [2], parachute [3], pilot seat [4], anti-penetration structures [5], propulsion testing [6], and ultrasonic aerodynamic tests [7]. The main difference of this system from the missile test is its direct movement on the rails until it reaches the target. Slippers are used to truck the system on rails. The slippers slide on the rails to allow the sled to move. A real example of a sled is shown in “Fig. 1”.

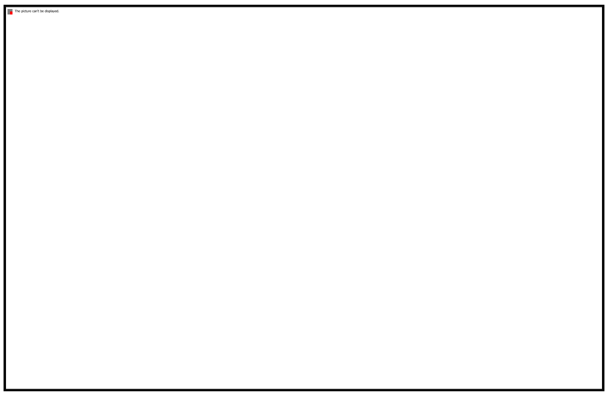

Fig. 1 Real examples of the sled system.

Sled testing technology has attracted the attention of researchers in recent years [8–12]. Impacts from engine propulsion, aerodynamic forces, as well as the impact of slippers on the rails cause significant vibrations to enter the sled structure [13]. Reduction of vibrations on the sled is one of the main problem in this system due to the high-speed motions, that has been attended by many researchers [14–17]. Xiao et al. used a one-degree-of-freedom system for modal analysis of a sled and obtained a damping ratio and mass stiffness matrix, then investigated the natural frequencies of the system using numerical methods [18]. Hauser showed that the vibrational environment in the sled test is a linear function of velocity. He mentioned that the vibrations on the sled are reduced using a pair of rails [19]. Hooser and Hooser used foam to reduce the transmitted vibrations on the explosive material in the middle of the sled body and reported the reduction of vibrations [20]. Lamb developed a structural model of the Holloman sled test and showed that the movement of the sled at critical speeds causes the transmission of vibrations to the rail. This theory was represented through time-frequency analysis of accelerometer data [21]. The vibrations of a system are related to different reasons, which can be carefully examined to determine the main source of vibrations and the effective factors on them. The main reason for vibrations in the sled system is referred to slipper impact on the rail. Considering the sled as a damping system, obtaining damping and equivalent stiffness is one of the main parts of system design. Considering the distance between the surfaces of the slipper colliding with one of the upper, lower, or lateral surfaces of the rail, the resulted vibrations cause vertical or lateral shocks, respectively. Research has shown that most of the rail collisions with the slipper occur in the upper parts of the slipper. In other words, the lateral part does not collide with the rail considerably, and the collision of the lower parts of the slipper with the rail along the sled path can be neglected. The contact of the slipper with the rail in the lower points 1 and 6 is less than 5% and then reaches a maximum of 18%. Variations of applied force on the top of the rail of points 3 and 4 are shown in “Fig. 2” [22]. Turnbull et al. used cable dampers inside the body, as shown in “Fig. 3”, to reduce the vibrations on the sled body.

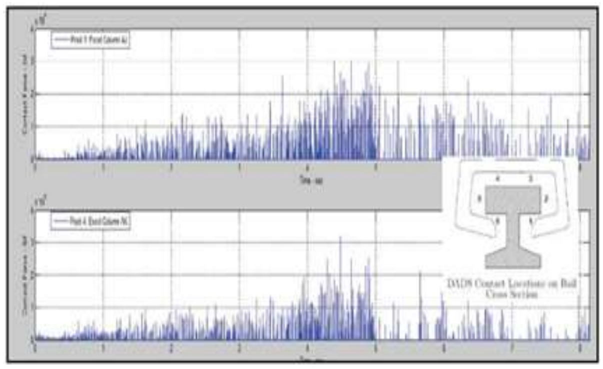

Fig. 2 Variation of the applied force on the top of the rail (points 3 and 4) [22].

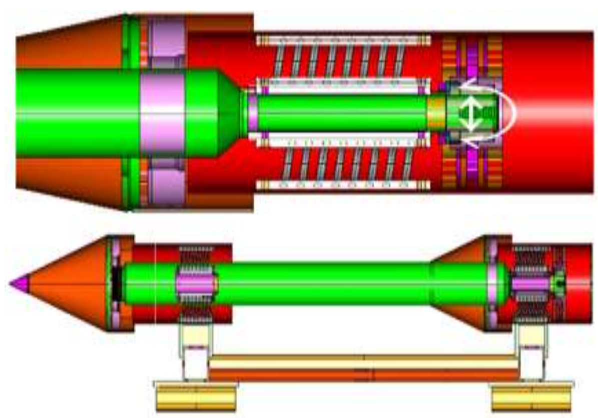

Fig. 3 Using Wire dampers to reduce vibrations [23].

The dampers were installed to withstand and reduce the torsional and vertical vibrations. The results showed that wire cable dampers greatly reduce vibrations in different directions [23]. Styrene-butadiene rubber (SBR), as composite [24-25] or constituent materials [26], is desirably used in damper to withstand against applied shocks due to better capabilities in comparison with springs[27]. SBR are one of the types of dampers that are identified in different types and applications [28]. The most important features of SBR elastomers are resistance to continuous cycles in terms of fatigue and failure, suspension of vibrations, reversibility against deflection and deformation, high flexibility against impact and shock, high displacement and flexibility capability along with a short distance, simultaneous performance of axial and lateral movements, no need for washers and seals, the ability to deform with low force and, by its nature, apply low force to equipment, low weight, and ease of installation and replacement [29]. In addition, to avoid the resonance phenomenon or reduction of vibration transmission in the system, the natural frequency can be increased by increasing the stiffness of the structure, but this makes the structure heavier and some difficulties for design of system[23]. The main outstanding of the present study, which has not been done by other researchers, is the use of structural elastomer dampers in the connection distance between the slipper and the sled body with a new method which a combination of analytical, numerical, and experimental test methods was utilized. Due to the importance of damping of vertical vibrations, the dampers are used to prevent the transmission of vibrations from the rail to the sled. In this research, SBR elastomer was selected as a novel idea for damping of system vibrations. First, by extracting the stiffness and damping Equations, the equivalent stiffness and equivalent damping of the system are obtained from a combination of analytical, numerical, and experimental methods, and by sled modal analysis, the natural frequency and the role of elastomer are investigated.

2 EQUIVALENT STIFFNESS EXTRACTION

Based on the aforementioned characteristics of SBR elastomer, it is used as a damper in the sled system. Considering the damper at the place where the slipper is attached to the sled body and considering the stiffness of the sled components, the rigidity of the elastomer used in the sled should be obtained.

2.1. Numerical Method

In this method, by obtaining the exact values of Young's modulus, Poisson's ratio, and elastomer density, using Abaqus software, different forces are applied to the part and the displacement of elastomer is obtained. Assuming the spring displacement is linear, the rigidity coefficient is obtained by dividing the amount of force on the displacement. What is available as the hardness coefficient of elastomers as an intrinsic property is their Shore factor. The hardness of materials is divided into two categories A and D based on the amount of Shore value. In our work, the elastomer of type A was selected. To obtain the stiffness of an elastomer, Young's modulus (E_e) should be obtained according to its stiffness value and then calculate its stiffness coefficient according to its geometry [30]. Young's modulus can be determined according to Equation (1) [31].

$$E_e = e^{(0.0235\ (\text{Shore,A}) - 0.6403)} \tag{1}$$

A hardness test was carried out to obtain the elastomer stiffness. This device is shown in “Fig. 4”.

Fig. 4 Hardness Tester.

By measuring the elastomeric shore value and substitution in Equation (1), Young's modulus is obtained. The density was measured equal to 1120 kg/m^3 by obtaining the weight of the elastomer, geometric dimensions and was compared with [32]. By entering different parameters in Abaqus software, the simulation is run. Finally, by entering these values in Abacus software, modeling is done. The number of meshes is 21985 and a type of quad element was selected. In this case, only rectangular elements are used to network and create the finite element network. The element used is C3D8R. This element is in the form of 8 cubic nodes, has a reduced formulation, the ability to control the Hourglass phenomenon and is one of the most widely used elements used in Abaqus software. Fig. 5 shows the elastomer under force.

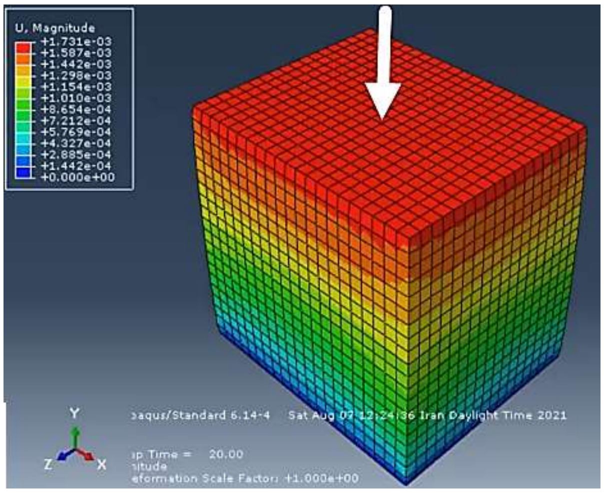

Fig. 5 Elastomer under vertical force.

Fig. **6** also shows the values obtained from the amount of elastomer displacement under different forces.

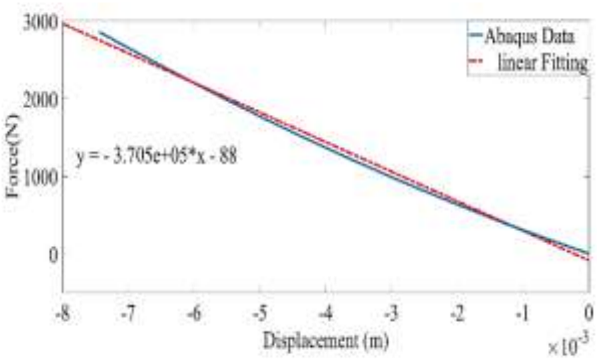

Fig. 6 Obtaining elastomer stiffness by applying different forces.

As can be seen, with increasing force (F) from 1 N to 3000 N, the vertical displacement (x) of the elastomer increases almost linearly. By extrapolating the results obtained from numerical simulation, the red dashed line is fitted to the blue line of Abaqus data, and the resulted Equation is described below

$$F= -370500x - 88 \tag{2}$$

The slope of the plot is equal to the amount of elastomer stiffness which is 370500 N/m.

2.2. Experimental Method

Harmonic dynamics test device was used to measure equivalent stiffness. This test was performed in Iran's spare parts manufacturing company, which is engaged in manufacturing various types of dampers and suspension systems for car manufacturing companies. The test apparatus is shown in "Fig. 7".

Fig. 7 Harmonic dynamics testing device of Iran spare parts manufacturing company.

The damper was fixed between plates, and a preload force was applied to prevent any gap between them. Next, the applied force to the elastomer and the resulted displacement is recorded and is monitored using the computer connected to the device. Fig. **8** shows the experiment performed at different frequencies and amplitudes of vibration.

Fig. 8 The harmonic dynamics testing device at the moment of applying force on the elastomer.

With the experiment, the elastomer stiffness was 391000 N/m that both experimental and numerical results are described in "Table 1". The values have a difference of less than 5% so the simulation results are confirmed.

Table 1 Amounts of experimental and numerical stiffness

Error percentage	Experimental stiffness (kN/m)	Numerical stiffness (kN/m)
5%	391	370.5

3 EXTRACTION OF EQUIVALENT DAMPING FACTOR

The present work contains a structural damping type. To obtain equivalent damping, we must first examine the vibrations with structural damping or hysteresis damping.

3.1. Obtaining Structural Damping Coefficient

When an object deforms, it absorbs and dissipates energy. The energy loss caused by friction between the inner planes and the material deforms is called structural or solid damping. In the case of stress-strain curves, the area of the closed hysteresis curve represents the dissipative energy in each cycle [33–35]. As shown in "Fig. 9", the area of this loop shows the dissipative energy due to structural damping for the unit volume of an object in a cycle [36].

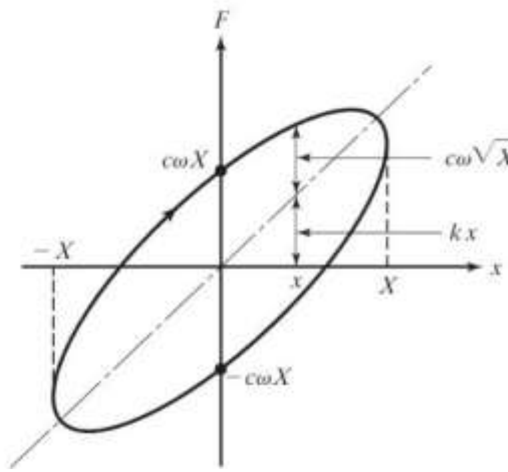

Fig. 9 force-displacement hysteresis loop.

Consider a system of one degree of freedom with structural damping capability as shown in "Fig. 10".

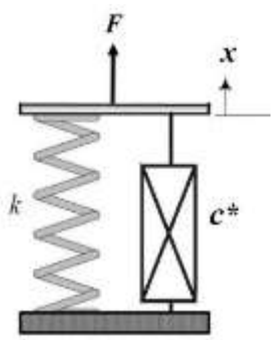

Fig. 10 One- degree of freedom system with structural damping capability.

The Equation of motion of the system is according to (3):

$$F = kx + c\dot{x} \tag{3}$$

Where, k relies on stiffness. Considering the harmonic motion, there is [37]:

$$F(t) = kx \pm c\omega\sqrt{X^2 - x^2} \tag{4}$$

Where, X is the amplitude of the vibration displacement. Thus, to obtain the amount of energy (ΔE_s), there is:

$$\Delta E_s = \int_0^{2\pi/\omega} (k\,X\sin\omega t \pm c\,X\cos\omega t)(\omega\,X\cos\omega t)dt = \pi\omega c X^2 \tag{5}$$

According to experiments, the energy loss per cycle is proportional to the stiffness of the material and the square of displacement and does not depend on the frequency [38]. To achieve damping behavior, we consider the damping coefficient c as follows [38]:

$$c = \frac{c^*}{\omega} \tag{6}$$

Where, c* is called the structural damping constant. Thus, using Equation (5), there is:

$$\Delta E_s = \pi c^* X^2 \tag{7}$$

With considering the parallel spring and damper, it can be obtained for harmonic motion $x = X\,e^{i\omega t}$ as the following Equation (8):

$$F = k\,X\,e^{i\omega t} + i\omega c\,X\,e^{i\omega t} = (k + i\omega c)\,x = (k + i\,c^*)\,x \tag{8}$$

Where, $k + ic^*$ is called mixed stiffness as Equation (9):

$$k + i\,c^* = k\left(1 + i\frac{c^*}{k}\right) = k(1 + i\,\beta) \tag{9}$$

The dimensionless constant β is called the structural damping ratio. Using Equation (7) the energy loss in a cycle can be written as Equation (10):

$$\Delta E_s = \pi\,\beta\,k\,X^2 \tag{10}$$

Since the value of ΔE_S is low, the motion can be considered harmonic. Referring to [39], equality of the energy stored in the spring and the energy loss value in a cycle, the constant amount of structural damping can be considered as a logarithmic reduction and defined as Equation (11):

$$\delta_1 = \ln \frac{X_1}{X_2} = \ln(1+\pi\beta) \cong \pi\beta \tag{11}$$

If the structure behaves similarly to one degree of freedom system, the damping ratio can be defined as (12) [40]:

$$\xi_{eq} = \frac{c_{eq}}{c_c} = \frac{c_{eq}}{2m\,\omega_n} \tag{12}$$

To determine the equivalent damping ratio, considering Equation (11), there is:

$$\xi_{eq} = \frac{\beta k}{2m\,\omega_n^{\,2}} = \frac{\beta}{2} = \frac{c^*}{2k} \tag{13}$$

On the other hand, the equivalent damping constant is obtained from Equation (14):

$$c_{eq} = 2\sqrt{k\,m}\,.\,\frac{\beta}{2} = \beta\sqrt{k\,m} = \frac{\beta k}{\omega} = \frac{\mathbf{c}^*}{\boldsymbol{\omega}} \tag{14}$$

Thus, considering Equation (13), there is:

$$\beta = \frac{2\delta_1}{\sqrt{4\pi^2 + \delta_1^{\,2}}} \tag{15}$$

3.2. Forced Movement of The System with Structural Damping

One degree of freedom system was considered with structural damping capability that is under the harmonic force as shown in “Fig. 11”.

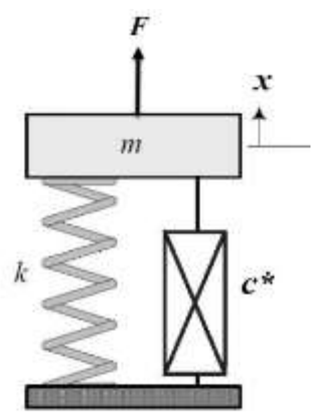

Fig. 11 One degree of freedom system with structural damping.

The Equation of motion of the system according to Equation (14) is obtained as Equation (16):

$$m\ddot{x} + \frac{\beta k}{\omega}\dot{x} + kx = F\sin\omega t \tag{16}$$

Where, the term of $((\beta\, k)/\omega)\,\dot{x}$ demonstrates the structural damping force. Considering the harmonic force, the stable solution of the Equation is considered to be as Equation (17):

$$x_p(t) = X\sin(\omega t - \varphi) \tag{17}$$

Thus, there is:

$$X = \frac{F}{k\sqrt{\left(1-r^2\right)^2 + \beta^2}} \tag{18}$$

$$\varphi = \tan^{-1}\frac{\beta}{1-r^2} \tag{19}$$

That term r of represent frequency ratio. According to experiments performed on materials and structures under harmonic load, it has been observed that the stress will exceed the strain by a constant angle δ. Therefore, for the harmonic strain $\varepsilon = \varepsilon_0.\sin(\omega t)$, the stress response is obtained as (20) [37]:

$$\begin{aligned} &\sigma(t) = \sigma_0\, sin(\omega t + \delta) = \\ &\sigma_0\, cos\delta\, sin\omega t + \sigma_0\, sin\delta\, cos\omega t = \\ &\sigma_0\, cos\delta\, sin\omega t + \sigma_0\, sin\delta\, sin\left(\omega t + \frac{\pi}{2}\right) \end{aligned} \tag{20}$$

The first term of Equation (20) is in the same phase with strain, while the second term of stress is 90 degrees with strain difference. By substituting $i = \sqrt{(-1)}$, there is [40]:

$$\sigma(t) = \sigma_0\, cos\delta\, sin\omega t + i\,\sigma_0\, sin\delta\;\; sin\omega t \tag{21}$$

With the definition of a composite module (E^*), there is:

$$E^* = \frac{\sigma}{\varepsilon} = \frac{\sigma_0}{\varepsilon_0} cos\delta + i\frac{\sigma_0}{\varepsilon_0} sin\delta \tag{22}$$

We define quantities of E' and E'' as storage modulus and waste modulus respectively, as is shown in Equations (23) and (24):

$$E' = \left(\frac{\sigma_0}{\varepsilon_0}\right) cos\delta \tag{23}$$

$$E'' = \left(\frac{\sigma_0}{\varepsilon_0} \right) sin\delta \tag{24}$$

So, Equation (25) is written:

$$E^* = E' + i E'' \tag{25}$$

Thus the stress response of linear viscoelastic materials to a harmonic strain input will be (26) [41]:

$$\sigma(t) = \varepsilon_0 \left(E' sin\omega t + E'' cos\omega t \right) \tag{26}$$

Where, ε_0 is the strain amplitude. The storage modulus is proportional to the average energy stored in a cycle, while the dissipation modulus is proportional to the average energy loss in a cycle [42]. The loss coefficient of η is dimensionless and is a measure of hysteresis damping in a structure, defined as (27) [41]:

$$\eta = \frac{E''}{E'} = tan\delta \tag{27}$$

The dissipation coefficient relates the wasted energy to the stored energy during the deformation cycle [43]. In other words, there is:

$$\frac{c^*}{k} = \eta \tag{28}$$

By substituting Equation (14) to (16), the free motion Equation of the system is obtained as (29):

$$m\ddot{x} + \frac{c^*}{\omega}\dot{x} + kx = 0 \tag{29}$$

Considering $x = X e^{i\omega t}$, there is:

$$\dot{x} = i\omega x \tag{30}$$

Therefore,

$$\frac{c^*}{\omega}\dot{x} = i c^* x \tag{31}$$

By using relations (31) and (29) there is:

$$m\ddot{x} + \left(k + i c^* \right) x = 0 \tag{32}$$

So, there is:

$$k + i c^* = k\left(1 + \frac{i c^*}{k} \right) = k\left(1 + i\eta \right) = k^* \tag{33}$$

Where, k is static stiffness and k* is complex stiffness. Finally, the Equation of motion is obtained as follows:

$$m\ddot{x} + k^* x = 0 \tag{34}$$

It describes that the combined effects of tensile strength, elasticity, and hysteresis capabilities can be represented as complex stiffness. Various experimental studies have been performed to obtain the loss coefficient. Environmental conditions such as temperature, type of test and are effective in determining the loss factor. “Table 2” shows the values of the loss coefficient η for SBR elastomer in various studies for ambient temperatures between 0 and 50 ° C.

Table 2 Loss coefficient values for SBR elastomer

SBR elastomer dissipation reference	Reference
0.2-0.3	[38]
0.15-0.45	[44]
0.18-0.36	[45]
0.22-0.4	[46]
0.15-0.4	[47]
0.28-0.12	[48]
0.05-0.45	[49]
0.1-0.3	[50]

Considering the obtained results, the value of the SBR loss coefficient decreased with increasing temperature in the range of 0 to 50 °C, so the range of 0.25-0.35 can be predicted for the SBR loss coefficient at 25 °C.

3.3. Experimental Test

An experimental test is used to obtain elastomer damping using the aforementioned dynamic test device. The elastomer under test is shown in “Fig. 12”.

Fig. 12 SBR elastomer dynamics test.

The procedure of the test is done by placing the elastomer in the device and adjusting it precisely to prevent from any distance between the device and the elastomer, so different frequencies were transmitted into the device which displayed the amount of tanφ at different frequencies. Considering Equation (19), tanφ is related to the two-dimensional value of the damping ratio of the structures, which can be expressed as following:

$$tan\varphi = \frac{\beta}{(1-r^2)} \tag{35}$$

The method for obtaining the natural frequency of elastomer was done first by designing the elastomer model in Abaqus software and entering the geometric characteristics and related parameters such as density and Poisson's ratio, the shape of elastomer different modes is obtained. Finally, due to the importance of vertical displacement of the elastomer in the present problem, the natural frequency of the elastomer is obtained using the results related to the mode shape. Considering the applied frequency value and the natural frequency of the elastomer, the frequency ratio of (r) is obtained, and the damping ratio of the structures can be obtained according to Equation (35) and the term of tanφ. The natural frequency of elastomer is shown in “Fig. 13”.

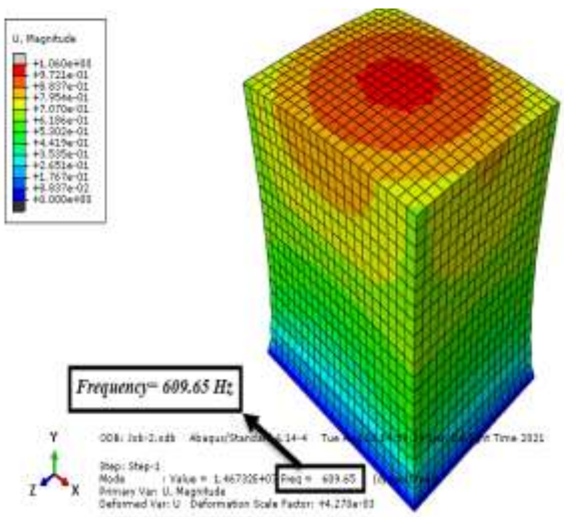

Fig. 13 Natural frequency of elastomer.

By substituting the values obtained in Equation (35), the value of β is extracted. “

Table **3**” shows the structural damping ratio of the system using experimental measurement of the phase difference between the force and displacement at different frequencies.

Table 3 Phase difference between force and displacement at different frequencies in the experimental experiment

β	tanφ	frequency
0.306	0.306	5
0.307	0.308	10
0.308	0.31	15
0.314	0.323	25
0.316	0.327	50
0.318	0.329	100

The differences between the mentioned values are negligible. The dimensionless value of the structural damping ratio is considered to be 0.31, and equivalent damping ratio (ξ_{eq}) is defined as:

$$\xi_{eq} = \frac{\beta}{2} = \frac{c^*}{2k} \rightarrow \xi_{eq} \cong 0.155 \tag{36}$$

Finally, by converting the unit of the natural frequency of the damper to radians per second and using Equation (14), the equivalent damping ratio is obtained as Equation (37):

$$c_{eq} = \frac{\beta k}{\omega} = \frac{0.31 \times 370000}{3830} = 29.94 \text{ N.s/m} \tag{37}$$

Considering the 25 grams weighs of the damper, the value of Ceq is validated, thus the loss factor values are compared. For this purpose, using Equation (14), the value of c^* is obtained as follows:

$$c^* = c_{eq}\ \omega = 29.94 \times 3830 = 114 \text{ kN.s/m} \tag{38}$$

Considering Eq. (38), the loss coefficient (η) is determined as following:

$$\eta = \frac{c^*}{k} \rightarrow \eta \cong 0.3 \tag{39}$$

The obtained results are in good agreement with the results of previous researches mentioned in “Table 2”, and the amount of equivalent damping is validated. By obtaining the equivalent damping and stiffness, the values of the various parameters of the sled, which determine the design parameters of the sled in our present work, are described in “Table 4”.

Table 4 Values of different parameters of the designed sled.

Parameter	Value	Unit
Sled mass	14.69	kg
Slipper mass	0.79	kg
Equivalent stiffness	370	kN/m
Second level torque	0.877	kgm^2
Equivalent Damping	29.01	N.s/m
Sled length	810	mm
Sled diameter	105	mm

4 SLED MODELING

Figure 14 represents the designed sled system and the dampers on the top of the slipper. The main body, which includes the propulsion and projectile engines, is considered as an integrated part, so two semi-circular rolled pieces, which are connected like a belt, are provided to restrain the main body. The dampers are connected from the bottom and top to the slipper and the belts, respectively. The belts are joined together with screws.

Fig. 14 Sled model.

4.1. Natural Frequencies and Shape of Modes

Fig. 15 shows the sled modal analysis for the first mode of the system. The first mode is related to the torsional vibrations around the center of mass of the sled. The first mode of the natural frequency is equal to 12.49 Hz. Due to the rigidity of the sled body, the amount of torsional vibration is small. The present condition demonstrates that one of the dampers is stretched and the other is under pressure.

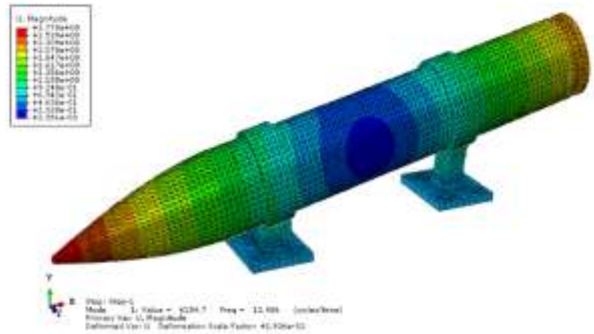

Fig. 15 The first (torsional) mode of the sled.

Fig. 16 shows the second mode of vibration which is related to the transverse vibration of the sled. In this case, the sled vibrates vertically without torsional motion, and the vibration rate of the two slippers is equal to each other. In this case, the second mode of the natural frequency is 19.56 Hz. The dampers are both stretched.

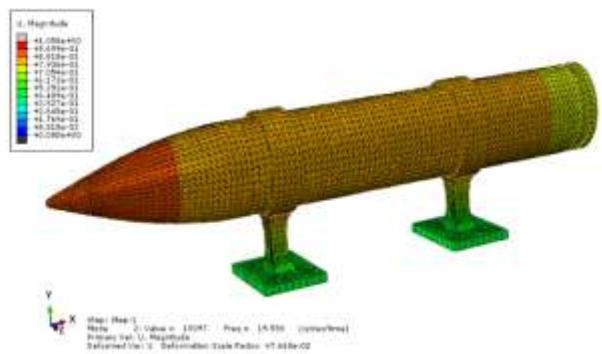

Fig. 16 Second (transverse) sled mode.

By examining the vibration modes and considering the rigidity of the sled body, the importance of the role of slippers in sled is determined that if the damper is not used, the vibrations will be transmitted to the sled body. Also, the use of elastomer dampers are the convenient choice because they can withstand pressure and tension, and do not transmit any displacement.

5 CONCLUSION

In this paper, the idea of using elastomer dampers to reduce the transmission of vibrations from the slipper to the sled body was investigated. First, by the relations governing the problem, equivalent stiffness and equivalent damping of the system were extracted from a combination of analytical, numerical, and experimental methods. So the stiffness values of 370500 and 391000 N⁄m were obtained numerically and experimentally. The difference between values was less than 5% so the results were confirmed. Then, by locating the damper and designing an example of a sled system, natural frequencies and system modes were obtained. The first and second modes of the natural frequency are equal to 12.49 and 19.56 Hz. The results showed the highest tension and pressure is applied on the dampers and elastomeric dampers prevent the transmission of vibrations and displacement of the sled body.

REFERENCES

[1] DeLeon, A., Palazotto, A. N., Shock Wave Investigation of High Speed Asperity Collision with Finite Element Modeling (January), 2020, pp. 1–20, Doi: 10.2514/6.2020-0316.

[2] Liu, J., Wang, W., and Zhao, F., Analysis of Wear for a Rocket Sled Slipper, MS&E, Vol. 398, No. 1, 12017, 2018.

[3] Gallon, J. C., Clark, I. G., Rivellini, T. P., and Adams, D. S., Witkowski A: Low Density Supersonic Decelerator Parachute Decelerator System, AIAA Aerodyn Decelerator Syst Conf, 2013, (March), 2013, pp. 1–14, Doi: 10.2514/6.2013-1329.

[4] Zhu, Y., Zhao, X., and Zhang, S., Computational Studies of Aircraft Life-Support Systems (January), 2011, pp. 1–16, Doi: 10.2514/6.2011-1045.

[5] Liu, Jun., Zhao, H., Gu, K., and Wang, W., An Analysis of Dynamic Response of a Rocket Sled. DEStech Trans Comput Sci Eng (aiea), 2017, pp. 956–67, Doi: 10.12783/dtcse/aiea2017/15034.

[6] Connell, T. L., Santi, S. A., Risha, G. A., Muller, B. A., and Batzel, T. D., Experiment and Semi-Empirical Modeling of Lab-Scale Hybrid Rocket Performance, 45th AIAA/ASME/SAE/ASEE Jt Propuls Conf Exhib (August), 2009, pp. 1–12.

[7] Doig, G., Barber, T. J., Leonardi, E., Neely, A. J., Kleine, H., and Coton, F., Aerodynamics of a Supersonic Projectile in Proximity to a Solid Surface, AIAA J, Vol. 48, No. 12, 2010, pp. 2916–30, Doi: 10.2514/1.J050505.

[8] Boardman, B., Uber, R., Baker, W., and Palazotto, A. N., Modeling Nonlinear Heat Transfer for Pin-on-Disc Sliding System, (January), 2020, pp. 1–22, Doi: 10.2514/6.2020-0973.

[9] Rodney, D., Gadot, B., Martinez, O., du Roscoat, S., Orge ´as L Reversible Dilatancy in Entangled Single-Wire Materials, Vol. 15, 2016, pp. 72–78.

[10] Tang, R. Y., Finite Element Structural Analysis of a Machine Gun Based on ANSYS, Nanjing Univ Sci Technol, 2007, pp. 17–37.

[11] Gao, W., Kessissoglou, N. J., Dynamic Response Analysis of Stochastic Truss Structures under Non-stationary Random Excitation using the Random Factor Method, Comput Methods Appl Mech Engrgy, Vol. 196, 2007, pp. 2765–73.

[12] Gerasimov, S. I., Erofeev, V. I., Calculation of Flexural-and-Torsional Vibrations of a Rocket Track Rail, J Mach Manuf Reliab, Vol. 45, No. 3, 2016, pp. 211–3.

[13] Liu, J., Wang, W., Zhao, F., and Gong, M., Comparison of Two Rocket Sled Slipper Materials for Resistance to Wear, AIP Conf Proc 1890(October), 2017, Doi: 10.1063/1.5005321.

[14] Hale, C. S., Palazotto, A. N., and Baker, W. P., Engineering Approach for The Evaluation of Mechanical Wear Considering the Experimental Holloman High-Speed Test Track, J Eng Mech, Vol. 138, No. 9, 2012, pp. 1127–40, Doi: 10.1061/(ASCE)EM.1943-7889.0000409.

[15] Shockley, J. A., Zetterstrom, S., 50 Years of The Central Inertial and GPS Test Facility, US Air Force T E Days 2009 (February), 2009, pp. 1–32, Doi: 10.2514/6.2009-1724.

[16] Zhang, J., Dynamic Coupling Analysis of Rocket Propelled Sled Using Multibody-Finite Element Method, Vol. 18, No. 4, 2014, pp. 25–30.

[17] Deleon, A., Baker, W. P., and Palazotto, A. N., Evaluation of a Nonlinear Melt Region Produced Within a High Speed Environment, AIAA/ASCE/AHS/ASC Struct Struct Dyn Mater Conf 2018 (210049), 2018, pp. 1–17, Doi: 10.2514/6.2018-0187.

[18] Xiao, J., Zhang, W., Xue, Q., Gao, W., and Zhang, L., Modal Analysis for Single Track Sled (Pmsms), 2018.

[19] Hooser, M., Soft Sled – The Low Vibration Sled Test Capability at The Holloman High Speed Test Track, 2018 Aerodyn Meas Technol Gr Test Conf (February), 2018, pp. 1–12, Doi: 10.2514/6.2018-3872.

[20] Hooser, M., Hooser, C., Soft Sled Design Evaluation Report, 2016.

[21] Lamb, J. L., Critical Velocities for Rocket Sled Excitation of Rail Resonance, Johns Hopkins APL Tech Dig Applied Phys Lab, Vol. 21, No. 3, 2000, pp. 448–58.

[22] Buentello Hernandez, R. G., Palazotto, A. N., and Le, K. H., 3D Finite Element Modeling of High-Speed Sliding Wear, Collect Tech Pap-AIAA/ASME/ASCE/AHS/ASC Struct Struct Dyn Mater Conf, 2013, pp. 1–20.

[23] Turnbull, D., Hooser, C., Hooser, M., and Myers, J., Soft Sled Test Capability at the Holloman High Speed Test Track. US Air Force T&E Days, 2010.

[24] Bahadar, A., Zwawi, M., Development of SWCNTs-Reinforced EPDM/SBR Matrices for Shock Absorbing Applications, Mater Res Express, Vol. 7, No. 2, 2020, pp. 025310, Doi: 10.1088/2053-1591/AB71CE.

[25] Liu, F., Zheng, M., Liu, X., Ding, X., Wang, F., and Wang, Q., Performance Evaluation of Waterborne Epoxy Resin-SBR Composite Modified Emulsified Asphalt Fog Seal, Constr Build Mater, Vol. 301, 2021, pp. 124106.

[26] Yang, L., Wang, L., Guo, H., and Du, A., Compressive Fatigue Behavior of Gum and Filled SBR Vulcanizates. Polymers (Basel), Vol. 13, No. 9, 2021, pp. 1497.

[27] Gil, A., Huang, A., Madrid, P., and Jiménez, L., Analysis of SBR Polymer Adapted to an Automobile Damping System, Journal of Undergraduate Research, Vol. 1, No. 2, 2015.

[28] Fu, Y., Kabir, I. I., Yeoh, G. H., and Peng, Z., A Review on Polymer-Based Materials for Underwater Sound Absorption, Polym Test, 2021, pp. 107115.

[29] Akyüz, S., Dari, M. E., Esiyok, Y. E., and Ermeydan, M. A., Effects of NR/SBR Ratio on Mechanical Properties and Artificial Mechanical Performance of Anti-Vibration Bushings, Iran Polym J, Vol. 30, No. 12, 2021, pp. 1317–28.

[30] Dudea-Simon, M., Dudea, S. M., Schiau, C., Ciortea, R., Mualuțan, A., Simon, V., Burde, A., Ciurea, A., and Mihu, D., Inter-and Intraobserver Reproducibility of Strain and 2D Shear Wave Elastography--a Phantom Study, Med Ultrason, 2021.

[31] Krmela, J., Material input for tire simulation, 2019.

[32] Asme, A., Ahs, A., Structures ASC, A01-25011 (c), 2001.

[33] Pinsker, W., Structural Damping, J Aeronaut Sci, 1949, pp. 699.

[34] Ungar, E. E., The Status of Engineering Knowledge Concerning the Damping of Built-Up Structures, J Sound Vib, Vol. 26, No. 1, 1973, pp. 141–54, Doi: 10.1016/S0022-460X(73)80210-X.

[35] Scanlan, R. H., Mendelson, A., Structural Damping, AIAA J, Vol. 1, No. 4, 1963, pp. 938–9, Doi: 10.2514/3.1684.

[36] Singiresu, S. R., and et al., Mechanical Vibrations, Addison Wesley Boston, Reading, MA, 1958.

[37] Chakraborty, Bikash Chandra Ratna, D., Polymer for Vibration Damping Appliction, 2020, pp. 348.

[38] Lazan, B. J., Damping of Materials and Members In Structural Mechanics, Pergamon Press LTD, Oxford, England, 1968, pp. 317.

[39] Orban, F., Damping of Materials and Members in Structures, Journal of Physics: Conference Series, Vol. 268, 2011, pp. 12022.

[40] Al-Gahtany, S. A., Mechanical Properties oof Styrene Butadiene Rubber-/Ethylene Propylene Diene Monomer Rubber-Based Conductive Blends, J Elastomers Plast, Vol. 45, No. 4, 2013, pp. 367–89, Doi: 10.1177/0095244312454035.

[41] Mohseni, A., Shakouri, M., Natural Frequency, Damping and Forced Responses of Sandwich Plates with Viscoelastic Core and Graphene Nanoplatelets Reinforced Face Sheets, JVC/Journal Vib Control, Vol. 26, No. 15–16, 2020, pp. 1165–77, Doi: 10.1177/1077546319893453.

[42] Schramm, G., A Practical Approach to Rheology and Rheometry, Hardcover – Illustrated, January 1, 1994.

[43] Riande, E., Díaz-Calleja, R., Prolongo, M. G., Masegosa, R. M., and Salom, C., Polymer Viscoelasticity : Stress and Strain In Practice, Boca Raton, 2014, pp. 904, https://doi.org/10.1201/9781482293241.

[44] Bahadar, A., Zwawi, M., Development of SWCNTs-Reinforced EPDM/SBR Matrices for Shock Absorbing Applications, Mater Res Express, Vol. 7, No. 2, 2020, pp. 25310.

[45] Araujo-Morera, J., Hernández Santana, M., Verdejo, R., and López-Manchado, M. A., Giving a Second Opportunity to Tire Waste: an Alternative Path for the Development of Sustainable Self-Healing Styrene-Butadiene Rubber Compounds Overcoming the Magic Triangle of Tires, Polymers (Basel), Vol. 11, No. 122019, pp. 2122.

[46] McKeen, L. W., The Effect of UV Light and Weather on Plastics and Elastomers, William Andrew, Hardcover ISBN: 9780128164570, 2019.

[47] Schaefer, R. J., Mechanical Properties of Rubber, Harris' Shock Vib Handbook, Sixth Ed A Piersol, T Paez (Eds), McGraw-Hill Co Inc, 2010, pp. 31–3.

[48] Mondal, D., Ghorai, S., Rana, D., De, D., and Chattopadhyay, D., The Rubber--Filler Interaction and Reinforcement in Styrene Butadiene Rubber/Devulcanize Natural Rubber Composites with Silica--Graphene Oxide, Polym Compos, Vol. 40, S2, 2019, E1559-E1572.

[49] Chakraborty, B. C., Ratna, D., Polymers for Vibration Damping Applications. Elsevier, Paperback ISBN: 9780128192528, 2020.

[50] Praveen, S., Chattopadhyay, P. K., Jayendran, S., Chakraborty, B. C., and Chattopadhyay, S., Effect of Nanoclay on The Mechanical and Damping Properties of Aramid Short Fibre-Filled Styrene Butadiene Rubber Composites, Polym Int, Vol. 59, No. 2, 2010, pp. 187–97.